ORGANOMETALLICS

pubs.acs.org/Organometallics

Article

Two Complementary Approaches to Silicon-Supported Soluble [FeFe]-Hydrogenase Mimics

Sergio Aguado, Diego J. Vicent, Luis Casarrubios,* Carmen Ramírez de Arellano, and Miguel A. Sierra*

Cite This: https://doi.org/10.1021/acs.organomet.2c00277

Read Online

ACCESS | Metrics & More | Article Recommendations | Supporting Information

ABSTRACT: Two series of silicon-supported [(μ-SCH_2)$_2$N^{R}Fe$_2$(CO)$_6$] (R = *p*-OHC_6H_4, **3**, and $(CH_2)_2OH$, **4a**, and $(CH_2)_5OH$, **4b**) hydrogenase mimics, as well as octamethylsilsesquioxane (POSS)-based nanostructures containing eight [(μ-SCH_2)$_2$N^{R}Fe$_2$(CO)$_6$] moieties, have been prepared either by reaction of the corresponding silyl and silyloxy chlorides and compounds **3** and **4** or by CuAAC between propargyl derivatives of silyl and silyloxy chlorides and azide **14**. Cycloaddition between POSS-derived azide **23b** and [(μ-SCH_2)$_2$N^{R}Fe$_2$(CO)$_6$] (R = alkyne) complexes **24** and **26** is efficient, leading to POSS-based nanostructures containing eight [(μ-SCH_2)$_2$N^{R}Fe$_2$(CO)$_6$] units. All of the complexes prepared through this work were soluble in organic solvents and hence fully characterizable by spectroscopic media. The electrochemistry of the linear siloxanes **6a** and **10** is similar, with a reduction wave around −1.7 V, which is characteristic of these [(μ-SCH_2)$_2$N^{R}Fe$_2$(CO)$_6$] entities. Complexes **6a** and **6b** lacking 1,2,3-triazole moieties were electrochemically stable in the presence of AcOH, showing a strong electrocatalytic wave at −2.2 V, while complexes **16** and **18** having the 1,2,3-triazole ring decomposed but were electrocatalytically active in the wave at −2.2 V. POSS-[(μ-SCH_2)$_2$N^{R}Fe$_2$(CO)$_6$] derivatives **25** and **27** show a strong irreversible reduction event and are deposited in the electrode either when adding AcOH or over time (successive voltammograms). ^{29}Si NMR shows that the integrity of the silicon cage is not affected by time or AcOH addition. These synthetic protocols and electrochemical studies will be applied in the design of silicon-supported [(μ-SCH_2)$_2$N^{R}Fe$_2$(CO)$_6$] mimics.

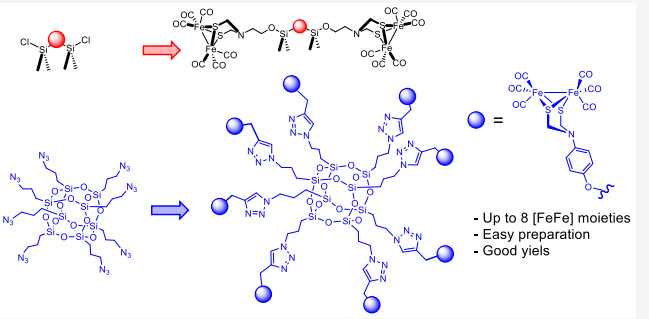

Downloaded via UNIV COMPLUTENSE DE MADRID on October 5, 2022 at 06:18:40 (UTC).
See https://pubs.acs.org/sharingguidelines for options on how to legitimately share published articles.

INTRODUCTION

Hydrogenase enzymes[1] are present in different organisms such as anaerobic bacteria or green algae. These enzymes have been targeted by researchers in search of new ways to produce energy due to their ability to reduce protons liberating molecular hydrogen (hydrogen evolution reaction, HER) as well as the inverse reaction, the oxidation of hydrogen to form protons. A plethora of studies[2] on the catalytic cycles of these enzymes has contributed to the design and obtention of non-enzymatic entities that mimic these natural substrates but lack oxygen sensitivity and thermal instability. A fair amount of the work done in the synthesis of hydrogenase mimics has been based on the preparation of complexes having [(μ-SCH_2)$_2$N^{R}Fe$_2$(CO)$_6$] or [Fe$_2$(μ-bdt)^R(CO)$_6$] (bdt = benzene-1,2-dithiolate) cores (Figure 1).[3] The incorporation of these metal complexes in different materials has also been profusely studied.

Thus, inclusion of mimics of [FeFe]-hydrogenases into TiO_2 surfaces,[4] nanotubes and nanocrystals,[5] metal−organic frameworks,[6] dendrimers,[7] polymers,[8] sodium dodecyl sulfate micellar systems,[9] nanocrystals,[10] and less frequent supramolecular assemblies[11] have been reported. In this regard, the anchoring of [FeFe]-hydrogenases into silica gel or doped silica gel (for example, with conducting metals) has been scarcely reported. A recent example shows that the silicon photoelectrode interface having covalently bonded [FeFe]-hydrogenase mimics photoelectrochemically generate hydrogen. However, after hydrolysis, loss of the [FeFe] moiety is also observed.[12] Several other silica-based heterogeneous systems have been used to immobilize [2Fe2S],[13] photo-

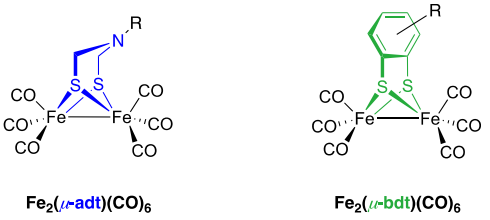

Figure 1. Different cores for the synthesis of hydrogenase mimics.

Special Issue: Organometallic Chemistry Inspired by Maurice Brookhart

Received: June 6, 2022

© XXXX The Authors. Published by American Chemical Society

sensitizer-[2Fe2S],[14] and other diiron complexes. In all cases, an improvement in the stability of the complexes and in their catalytic activity was observed.[3c]

However, homogeneous silicon-containing [FeFe]-H_2-ase mimics have been less studied. The only described family of silicon-containing hydrogenase mimics are those where the nitrogen of the adt bridge is exchanged with a silicon atom (Figure 2), having a silicon bridging moiety between the two sulfur atoms instead of the nitrogen present in the natural hydrogenase.[15,16]

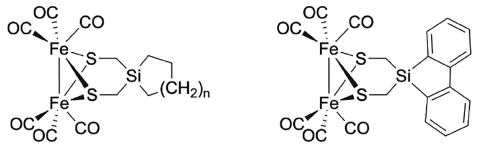

Figure 2. Soluble Si-containing [FeFe]-H_2-ase mimics.

These analogues of the natural active center of [FeFe]-hydrogenases were prepared based on the hypothesis that the properties of the mimic would be different from their nitrogenated or carbon-based analogues. Especially relevant was the idea that silicon could be important in the protonation of the sulfur bridges, as they have been proposed as possible basic positions during the catalytic hydrogen-producing reactions in a [FeFe]-hydrogenase mimic. In fact, the first μ-protonation in a sulfur atom having a bridging silicon was reported in 2010,[17] and since then, several complexes of these classes have been prepared.

Additionally, functionalized silicon bridges have been used as a support for [FeFe] mimics as antennas in light-driven H_2 production[18] However, the synthesis of siloxanes and polysiloxanes including several subunits of $[(\mu\text{-}SCH_2)_2N^RFe_2(CO)_6]$ and soluble organic solvents has not been reported to date. We describe herein two complementary methods to prepare silanes and siloxanes of increasing complexity, including octamethylsilsesquioxanes (POSS) derivatives, with the common feature is being soluble in organic solvents and hence characterizable by spectroscopic techniques. The electrochemistry and electrocatalytic properties of these compounds containing up to eight [FeFe] units will also be reported.

RESULTS AND DISCUSSION

The first approach to silicon derivatives containing up to four silicon atoms was developed using the reaction of chlorosilanes and $[(\mu\text{-}SCH_2)_2N^RFe_2(CO)_6]$ (R = p-OHC_6H_4, **3**, and $(CH_2)_2OH$, **4a**, and $(CH_2)_5OH$, **4b**) mimics. Thus, diphenydichlorosilane was reacted with cluster **3** in the presence of Et_3N in ether at 0 °C, yielding tetranuclear complex **5** having two [FeFe] units in 52% yield after SiO_2 chromatography. Complexes **6** having aliphatic chains (two and five CH_2 groups) were obtained in 53 and 56% yields. Complexes **5** and **6** were stable compounds and were characterized by spectroscopic means (Scheme 1). Especially relevant was the ^{13}C NMR signal at 207.1 ppm for **5** and 207.7 and 207.9 ppm for **6a** and **6b**, respectively, showing the presence of six equivalent CO ligands. The sole signal of ^{29}Si at −37.4 ppm for **5** and −20.1 and −32.2 ppm for **6a** and **6b**, respectively, together with the observed mass in the ESI-HRMS experiments (see experimental data for compounds **5**, **6a**, and **6b**) confirms the incorporation of two equivalent [FeFe]-containing units. This analysis (^{29}Si NMR together with ESI-HRMS) was extended to confirm the structures of all of the products incorporating several units of the [FeFe] moiety along this work. Moreover, integration of a well-resolved signal of the $NSCH_2$ protons versus the specific protons at the silicon linkers can also be used to determine the number of [FeFe]-incorporated units. Additionally, the structure of complex **5** was unambiguously determined by single-crystal X-ray diffraction analysis (Figure 3). The structure shows a diphenylsilanediyl ligand bridging two $[(\mu\text{-}SR)_2Fe_2(CO)_5]$ units with a [2Fe2S] cluster adopting a butterfly geometry. In the iron clusters, the N-substituted azadisulfide bridging ligand and both iron atoms form two fused six-membered metallocycles. The metallocycles corresponding to Fe(2) and Fe(3) adopt a boat conformation with Fe(2)···N(1) and Fe(3)···N(2) distances of 3.415(2) and 3.497(4) Å, respectively. The Fe−Fe bond lengths (2.4989(5) and 2.5113(5) Å) lie in the range found for similar μ-(phenylazanediyl)bis-(methanethiolate) diiron structures (2.489−2.595 Å). (Figure 3).[19]

Scheme 1. Synthesis of Silanes 5 and 6

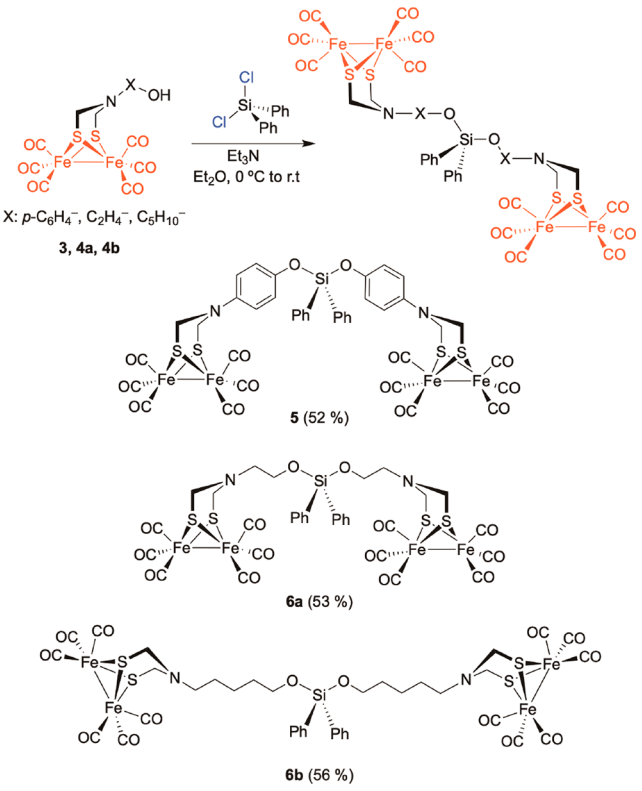

Following a similar approach, dichlorodisiloxane **7** and dichlorotetrasiloxane **8** were reacted with aliphatic alcohol **4a**, yielding the corresponding tetranuclear compounds **9** and **10** in 48 and 55% yield, respectively, after purification by SiO_2 chromatography (Scheme 2). ^{29}Si was essential to prove the homogeneity of the prepared products. Thus, complex **9** gave one signals at −10.95 ppm corresponding to the two equivalent silicon atoms attached to the chains bearing the clusters. In turn, complex **10** having two non-equivalent silicon atoms showed the two expected signals at −11.63 ppm for the central Si atoms and −21.11 ppm for those attached to the

https://doi.org/10.1021/acs.organomet.2c00277
Organometallics XXXX, XXX, XXX−XXX

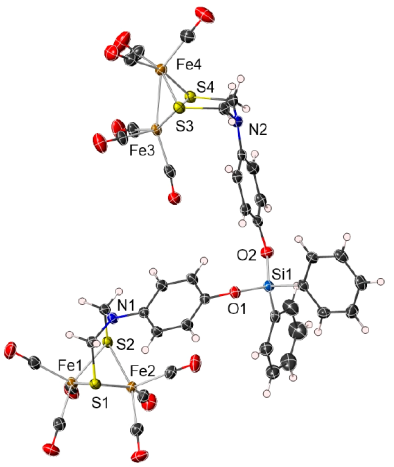

Figure 3. X-ray thermal ellipsoid plot of **5** (50% probability level) with the labeling scheme. Selected bond lengths (Å) and angles (deg): Fe(1)−S(2) 2.2691(7), Fe(1)−S(1) 2.2733(7), Fe(1)−Fe(2) 2.4989(5), Fe(2)−S(2) 2.2585(7), Fe(2)−S(1) 2.2701(7), Fe(3)−S(3) 2.2646(7), Fe(3)−S(4) 2.2684(7), Fe(3)−Fe(4) 2.5113(5), Fe(4)−S(3) 2.2692(7), Fe(4)−S(4) 2.2695(7), Si(1)−O(2) 1.6387(18), Si(1)−O(1) 1.6477(18), S(2)−Fe(1)−S(1) 84.32(2), S(2)−Fe(2)−S(1) 84.64(2), S(3)−Fe(3)−S(4) 85.62(2), S(3)−Fe(4)−S(4) 85.49(3), Fe(2)−S(1)−Fe(1) 66.73(2), Fe(2)−S(2)−Fe(1) 67.00(2), Fe(3)−S(3)−Fe(4) 67.27(2), Fe(3)−S(4)−Fe(4) 67.20(2), O(2)−Si(1)−O(1)111.54(10).

Scheme 2. Synthesis of 9 and 10

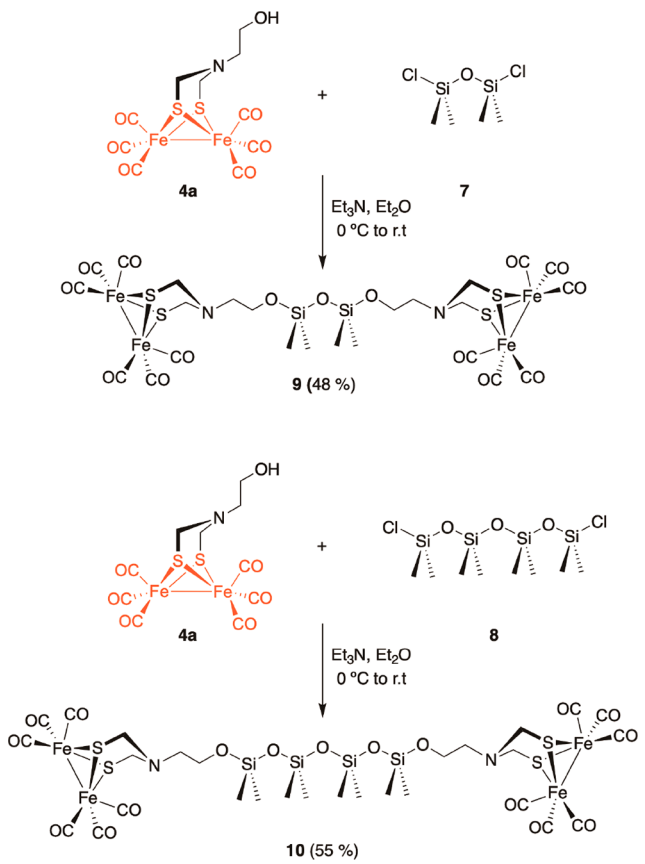

cluster chains. Complexes **9** and **10** show a single signal attributable to the CO ligands in their ^{13}C NMR spectra at 207.9 and 208.0 ppm, respectively, showing the equivalence of the 12 CO ligands attached to the four Fe centers. The IR spectrum of complex **9** consists of three characteristic bands at 2071, 2027, and 1985 cm^{-1}, similar to related reported complexes (Table 1).[20]

Table 1. Data of ^{13}C, ^{29}Si, and IR (ν_{CO}) for Siloxane Derivatives and Triazole-Derived Complexes 5−22

	^{13}C NMR (ppm)	^{29}Si NMR (ppm)	ν_{CO} (cm^{-1})
5	207.1	−37.40	2073, 2031, 1993
6a	207.7	−30.10	2071, 2027, 1989
6b	207.9	−32.20	2071, 2028, 1990
9	207.9	−10.95	2071, 2027, 1985
10	208.0	−11.63, −21.11	2072, 2029, 1990
11	207.8	−57.50	2071, 2028, 1967
13	207.1	−37.40	2071, 2028, 1971
16	206.9	−31.49	2071, 2028, 1967
18	206.9	−31.80	2074, 2032, 1993
20	206.9	−9.72	2073, 2029, 1984
22	206.9	−8.05	2074, 2030, 1989

The protocol developed above made it possible to join alcohol chains containing a $[(\mu\text{-}SCH_2)_2N^RFe_2(CO)_6]$ to silicon frameworks containing from one to four Si atoms. Depending on the number of halogen atoms in the starting silyl-derived chlorides, a maximum of three [FeFe] moieties (Scheme 3) have been attached to the silicon atom (so far, the reaction of $SiCl_4$ with alcohols or phenol complexes did not yield the desired products, as only complex decomposition reaction mixtures were observed). Finally, following this approach, we incorporated an electroactive moiety to the silicon atom using (dichloromethylsilyl)ferrocene **12**[21] and phenol **3** (Scheme 4). Complex **13** was obtained in 48% yield

Scheme 3. Synthesis of Complex 11

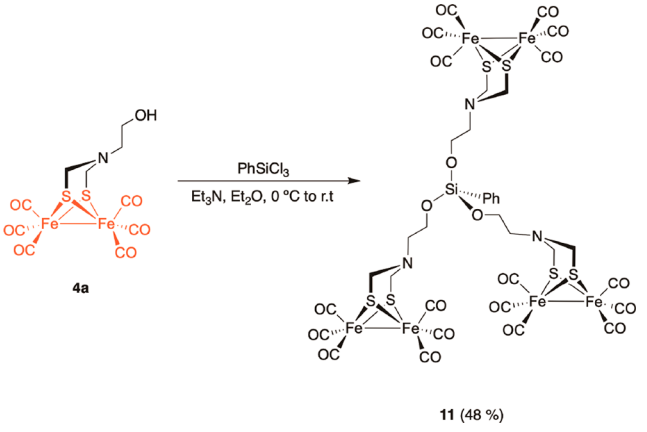

after SiO_2 chromatography. Again, the spectroscopic and HRMS data confirm the proposed structure, with a single signal attributable to the CO groups in the ^{13}C NMR spectra at 207.1 ppm and a single signal at −37.4 ppm in the ^{29}Si NMR spectra (Scheme 4). The IR spectrum of complex **13** shows CO bands similar to those of the previous complexes (**5**, **6a**, **6b**, **9**, **10**, and **11**; see Table 1) with shifts at 2071, 2028, and 1971 cm^{-1}.

We then turned our attention to the combination of this approach with the Cu-catalyzed azide alkyne cycloaddition. In fact, by preparing alkyne-substituted silyl and siloxane derivatives and subsequent reaction of these compounds with

https://doi.org/10.1021/acs.organomet.2c00277
Organometallics XXXX, XXX, XXX−XXX

Scheme 4. Synthesis of 13

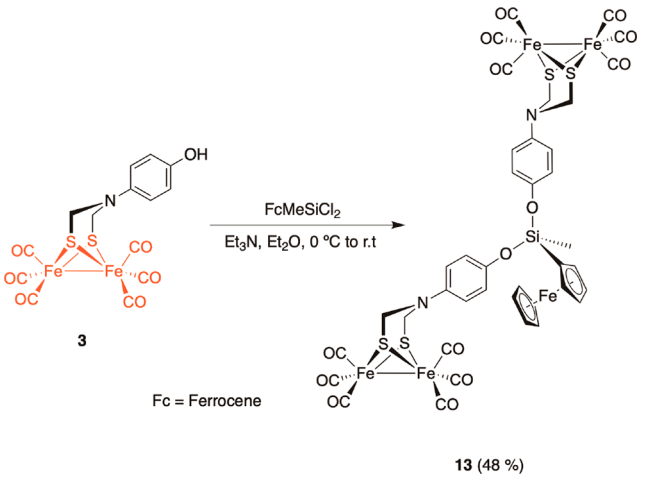

azide **14**, more sophisticated structures could be accessed. Thus, silyl derivatives **15** and **17** having alkyne substituents were prepared by reaction of the corresponding alcohols and diphenyldichlorosilane (see the Supporting Information (SI)). Compound **15** was reacted with azide **14** following our reported reaction conditions.[22] Bistriazoles **16** were obtained in good to excellent yields (Scheme 5). Together with the

Scheme 5. Synthesis of Complexes 16 and 18 by CuAAC

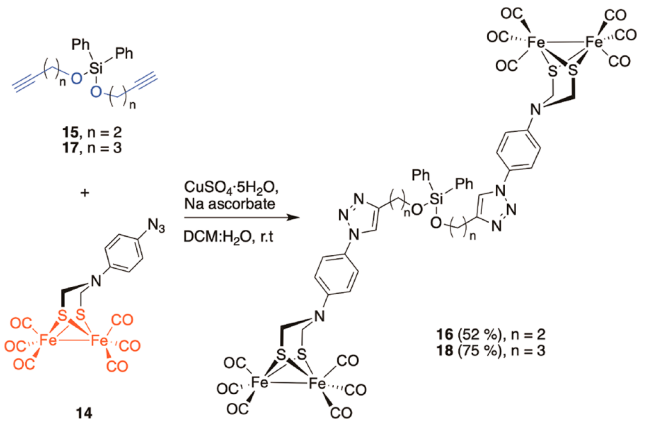

resonances assignable to the CH_2 groups, a signal at 7.86 ppm, characteristic of the CH of the 1,2,3-triazole moiety, confirmed the formation of the symmetric bistriazole derivative. The remaining spectroscopic and HRMS spectra confirmed the structure of compounds **16**.

Analogously, the reaction of 1,3-dichloro-1,1,3,3-tetramethyldisiloxane with propargylic alcohol produced disiloxane **19** that reacted nicely with azide **14** to form complex **20** in 87% yield. ^{29}Si NMR spectra of disiloxane **20** had a sole signal at −9.72 ppm, which together with the experimental value of HRMS (1250.7983) is consistent with the proposed symmetric structure of the siloxane. Conversely, the ^{13}C NMR spectra of complex **20** presented a single signal at 206.9 ppm attributable to the 12 equivalent CO ligands. Finally, we tested the possibility of including an electroactive moiety attached to the silicon. Thus, (dichloromethylsilyl)ferrocene was reacted with propargyl alcohol under the usual conditions, and the obtained ferrocenylmethyl-bispropargyl siloxane **21** was reacted with azide **14**. Complex **22** was obtained in 78% yield (Scheme 6).

The spectroscopic and HRMS data for compound **22** were consistent with the expected symmetric structure (Scheme 6).

Scheme 6. Synthesis of Complexes 20 and 22 by CuAAC of Alkynes 19 and 21 with Azide 14

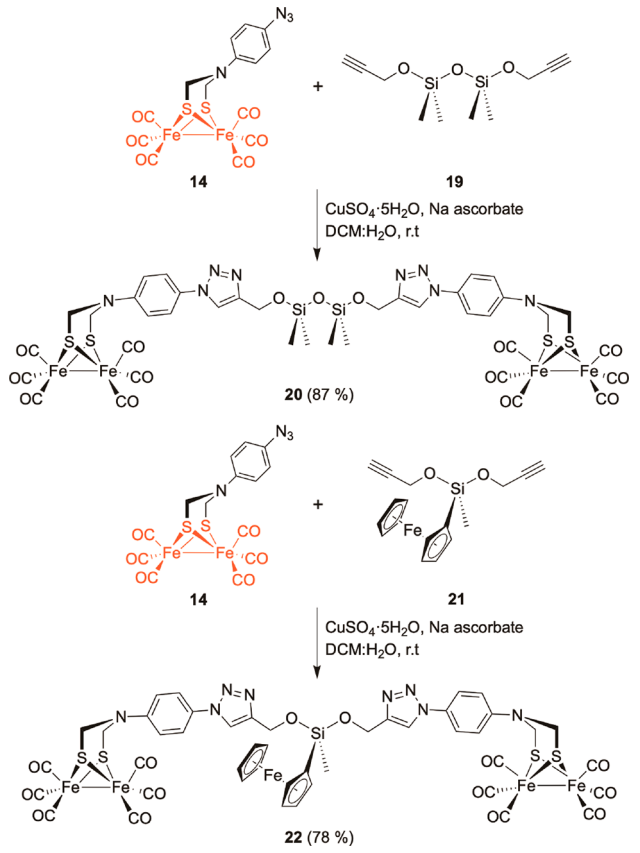

The ^{13}C shift values are identical in all complexes having the 1,2,3-triazole (206.9 ppm), as are the CO stretching band shifts in the IR spectra (differences of ν_{CO} = 3 cm^{-1}) (Table 1), showing that the electronic influence does not depend on the different silicon fragments, and the electron density around the FeFe core is very similar for the complexes having the 1,2,3-triazole.

Once the efficiency of the CuACC to prepare diverse silicon-supported [FeFe]-H_2-ase mimics was demonstrated, we tested our procedure with alkyne-POSS derivative **23a**.[23] Octamethylsilsesquioxanes are nanosized stable tridimensional structures having alternate Si−O bond forming cage structures with Si atoms in the vertices.[24] These compounds have unique characteristics and are exceptional building blocks to prepare hybrid materials.[25] Moreover, these compounds are suitable for functionalization using different catalytic reactions, including Heck,[26] metathesis,[27] and others.[28]

The reaction of **23a** and azide **14** (Scheme 7) led to a product which showed the characteristic triazole proton signal at 8.50 ppm, the AB aromatic system, and the methylene groups bonded to the sulfur atoms in a DMSO-d_6 ^{1}H NMR experiment (see the SI Figures S79 and S80). However, due to the extremely low solubility, we were not able to perform further experiments to fully characterize this product, and consequently, the electrochemistry of this product could not be performed either. Therefore, we modified our approach by inverting the position of the reactive functional groups, namely,

https://doi.org/10.1021/acs.organomet.2c00277
Organometallics XXXX, XXX, XXX−XXX

Scheme 7. Reaction of 14 and POSS Derivative 23a

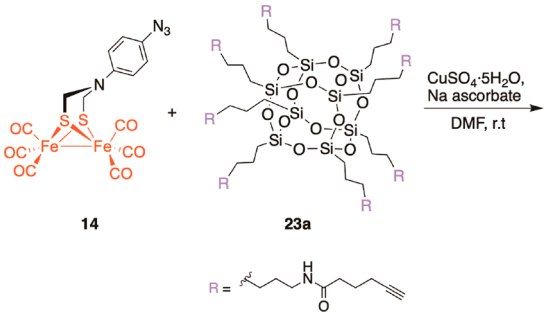

using the POSS azide **23b**[29] and the alkynylphenyl-substituted cluster **24**.[30] When these reagents were submitted to the standard CuACC conditions ($CuSO_4·5H_2O$, sodium ascorbate in a 1:1 mixture of DCM/water), the desired product, POSS **25** containing eight [FeFe] units, was obtained in 74% yield after purification by column chromatography (Scheme 8). The structure and homogeneity of the proposed POSS cluster was demonstrated by ^{29}Si NMR. In fact, a single signal was observed at −67.2 ppm. Additionally, a single signal corresponding to the CO ligands appeared at 207.1 ppm, as expected for the highly symmetric POSS nanocage. These data, together with the remaining NMR data and the combustion analysis, ensured the structure of POSS **25**.

Subsequent, POSS-azide **23b** was reacted with [FeFe] cluster **26** under analogous reaction conditions (Scheme 8). The desired POSS derivative **27** was obtained in 88% yield after SiO_2 chromatography, showing again regular disposition of the incorporated substituents (single signal in the ^{29}Si NMR at −67.3 ppm). The remaining spectroscopic and analytical data confirmed the structure of this compound.[31]

ELECTROCHEMISTRY

The electrochemical behavior of silyl derivatives **5**, **6**, **11**, and **13**, siloxane derivatives **9** and **10**, and complexes **16**, **20**, and **22** containing triazole derivatives was similar (Figures S1−S9). Thus, these compounds display a quasi-reversible wave in the range of −1.70 V (Table 2). This wave is attributed to the

Table 2. In All Cases, Data (V) Were Obtained from 10^{-3} M MeCN Solutions Containing 0.1 M $[N(^nBu)_4]PF_6$ as Supporting Electrolyte at 25 °C[a]

	E_{pc1}	E_{pa1}	$E_{(1)}$	I_{pa}[b]	I_{pc}[b]	TOF_1[c]	TOF_2[d]
5	−1.73	−1.59	−1.66	4.6	−30.6	0.4	17.5
6a	−1.72			1.7	−38.6	0.5	11.5
6b	−1.70	−1.67	−1.68	3.1	−30.5	0.5	11.5
10	−1.71	−1.66	−1.68	1.3	−35.7	0.5	10.4

[a]Potentials are given relative to $Fc^{0/+}$. Data are taken from Figure 4 and Figures S2, S3, and S5. [b]Data in μA. [c]TOF_1 first wave (s^{-1}). [d]TOF_2 second wave (s^{-1}).

Scheme 8. Synthesis of POSS Derivatives 25 and 27

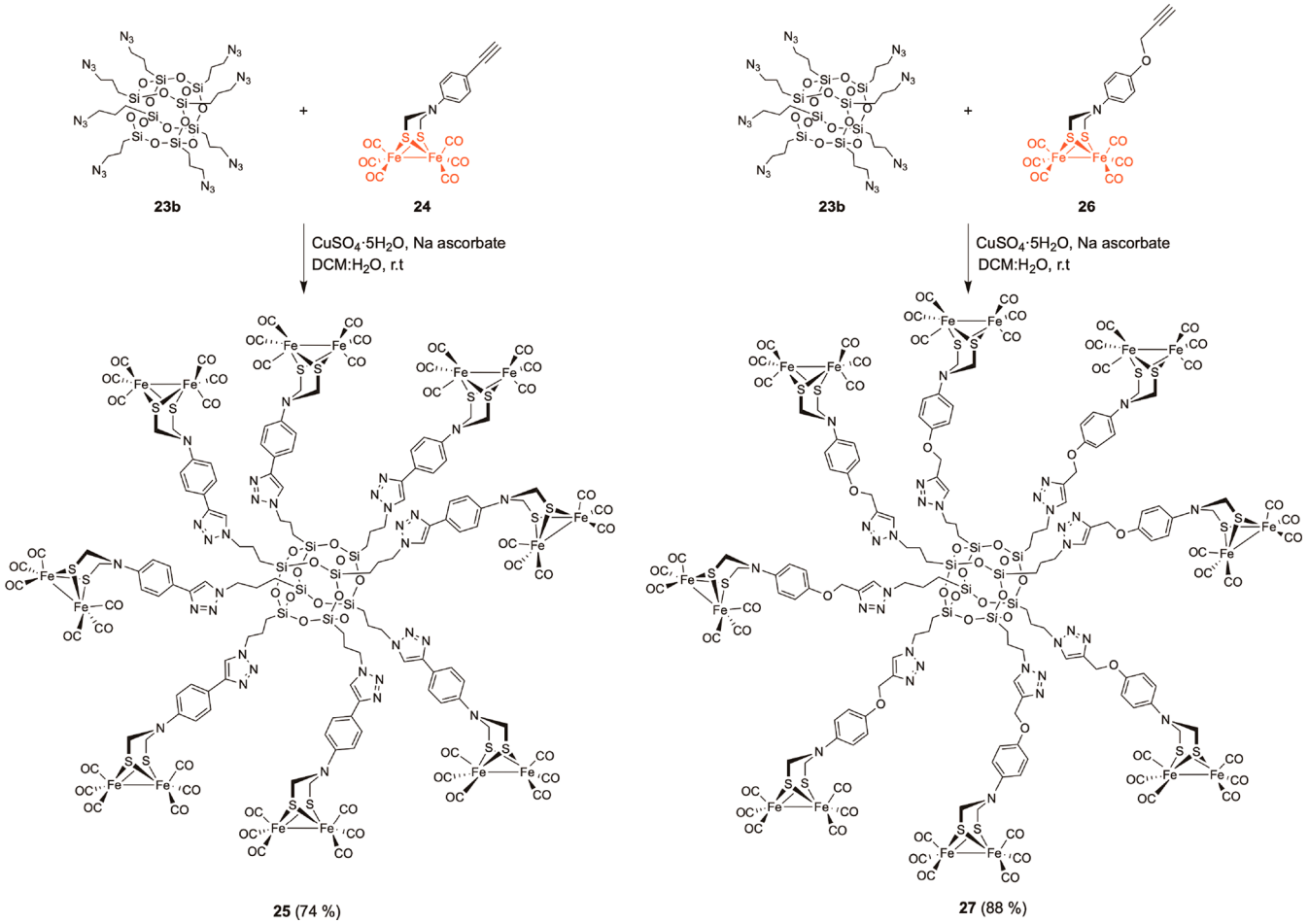

https://doi.org/10.1021/acs.organomet.2c00277
Organometallics XXXX, XXX, XXX−XXX

reduction of $[Fe_IFe_I]$ to $[Fe_IFe_0]$.[32] Analogously, a quasi-reversible oxidation wave appears at 0.50 V. This wave has been assigned to the $[Fe_IFe_I]$ to $[Fe_IFe_{II}]$ oxidation.

Figure 4 shows scan-rate-dependent cyclic voltammograms (CVs) of complex **13**. To calculate the experimental electron

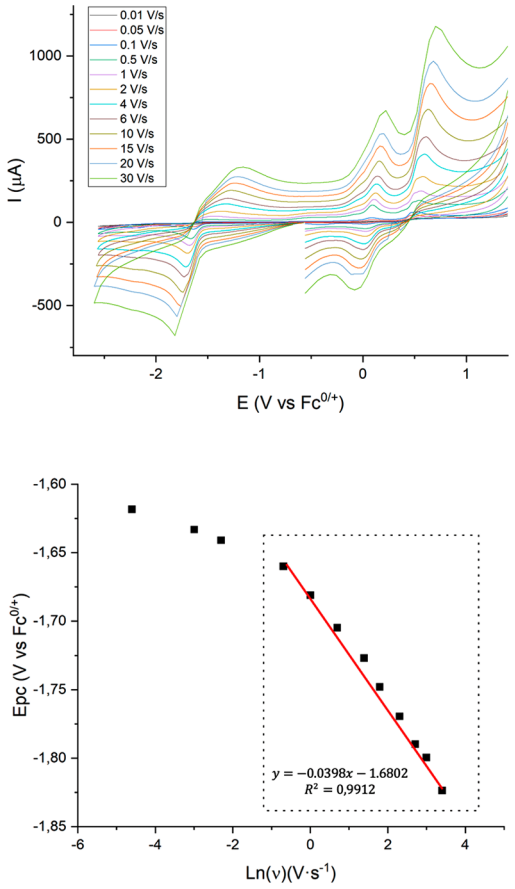

Figure 4. (Top) Scan-rate-dependent CVs of complex **13**. Data (V) obtained from 10^{-3} M MeCN solutions, containing 0.1 M $[N(^nBu)_4]PF_6$ as supporting electrolyte at 25 °C. (Bottom) E_{pc} versus $\ln(\nu)$ for complex **13**. The purely kinetic region is shown inside the black square.

transfer coefficient (α), the slope of the kinetic zone of the reversible wave attributable to the ferrocene ligand was used ($E_{1/2} \approx 0$ V versus Fc^0 (see SI Figure S19). Our experimental value for the electron transfer coefficient ($\alpha = 0.58$) allowed calculation of the number of electrons involved in the quasi-reversible wave at −1.70 V for complex **13** (eq 1).[33] Therefore, this wave implies a two-electron reduction process.

$$\frac{\partial Epc}{\partial \ln(\nu)} = \frac{2.3RT}{\alpha nF} = -39.8 \text{ mV when } n = 2 \quad (1)$$

The similarities in the electrochemical behavior of silicon-containing complexes prepared above disappear in the presence of AcOH. Thus, while complexes **6a** and **10**, lacking a triazole moiety in their structures, were stable against increased amounts of AcOH, the complexes having the 1,2,3-triazole moiety show a structure-dependent stability. Figure 5 depicts the voltammograms of silane **6a** in the presence of up to 20 equiv of acetic acid. Like other [FeFe] mimics, a negligible increase in current intensity in the wave centered at

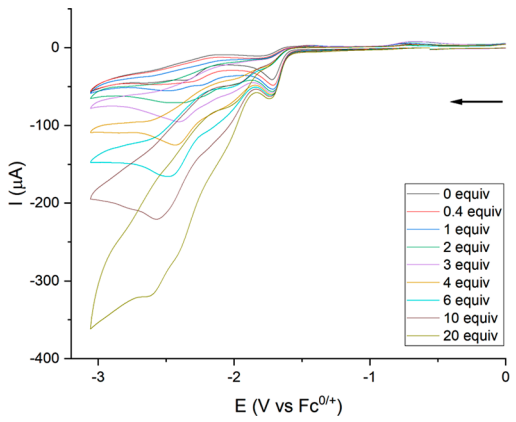

Figure 5. Cyclic voltammograms of **6a** with added AcOH (0−20 equiv of H^+). Data (V) obtained from 10^{-3} M MeCN solutions, containing 0.1 M $[N(^nBu)_4]PF_6$ as supporting electrolyte at 25 °C.

−1.70 V was observed, while a second wave at −2.30 V increases, showing a standard electrocatalytic response.[34]

The calculated turnover frequencies (TOFs) for these complexes are shown in Table 2 and Figure 6. The values of

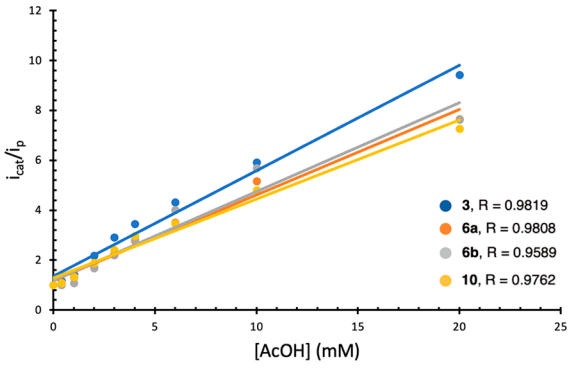

Figure 6. Plot of i_{cat}/i_p versus $[(AcOH)H^+]$ for the second wave for **3**, **6a**, **6b**, and **10**.

i_{cat}/i_p versus acid concentration show a first-order dependence in all cases. The observed rate constant does not become independent of acid concentration in the recorded values (up to 20 equiv of AcOH). Higher acid concentrations were not studied due to catalyst decomposition.

Upon addition of AcOH, triazole-containing complexes **16** and **18** showed a clearly different behavior. Thus, these two complexes having the 1,2,3-triazole moiety separated from the Si−O bond by two or three CH_2 groups experience a continuous decrease in the current intensity of the wave centered at −1.65 V when increasing the amount of AcOH, and simultaneously the intensity of the wave at −2.20 V (Figure S14) varies randomly. This could only be explained by a structural change in the molecule since neither electrode deposition nor apparition of insoluble material was observed while increasing the amount of acid.

To understand this differential behavior, the ^1H NMR in CD_3CN in the presence of variable amounts of AcOH was registered for complex **16**. This complex has the 1,2,3-triazole moiety separated from the Si−O bond by two CH_2 groups. The instantaneous formation of a new complex was observed in the presence of acetic acid. This new complex lacks the aromatic hydrogen attributable to the 1,2,3-triazole moiety

https://doi.org/10.1021/acs.organomet.2c00277
Organometallics XXXX, XXX, XXX−XXX

while maintaining the [FeFe] moiety (see SI Figure S81). In addition, we also observed a fast hydrolysis of complex **16** to the corresponding alcohol **16b** when ^{1}H NMR spectra were registered over time. The ^{13}C NMR of this new complex **16b** confirms the structure of the proposed alcohol (see SI Figure S47). Only the triazole complexes where the triazole is separated from the Si−O bond by one methylene group (**20** and **22**) were stable under these conditions.[35]

This fact pointed to a dependence of the distance between the triazole nucleus and the silicon center of the hydrolysis process. To elaborate on this hypothesis, complex **28** was prepared by reaction of azide **14** and TMS-acetylene (Scheme 9). Complex **28** was stable in the presence of increasing amounts of AcOH, showing the expected electrochemical behavior for these classes of compounds (Figure S13).

Scheme 9. Synthesis of 28

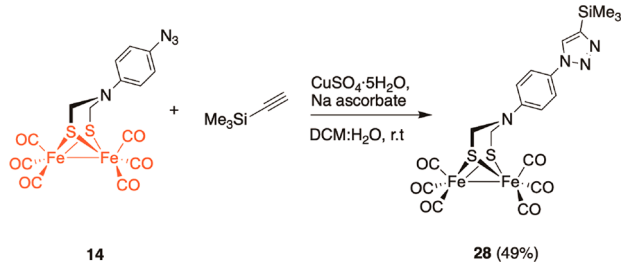

14 **28** (49%)

Finally, the electrochemical behavior against acid of POSS derivatives **25** and **27** was determined. These compounds showed an intense, irreversible, and sharp wave at −1.90 V, together with a strong and sharp irreversible oxidation wave at 0.90 V. The strong reduction response may be attributed to the simultaneous reduction of the eight [FeFe] units. Similarly, the strong oxidation response may be attributed to their simultaneous oxidation (Figures S15 and S16).

The cyclic voltammograms of POSS derivatives with a three-methylene linker between the triazole ring and the POSS units **25** and **27** show a clear disappearance of the electrochemical response in the presence of AcOH (Figure S17). However, in this case, a deposit of red material in the electrode was observed upon addition of 0.4 equiv of AcOH, pointing to a possible protonation of the POSS that would decrease its solubility, provoking the deposition in the electrode.

Nonetheless, ^{29}Si spectra of complex **27** were registered in CD_2Cl_2 in the presence of 3 and 10 equiv of acetic acid, and a single silicon signal was maintained in all cases (see SI Figure S83), demonstrating the stability of the octasubstituted complex in acidic conditions. The ^{1}H NMR in acidic media confirms these data (see SI Figure S82).

Furthermore, a similar effect (disappearance of the electrochemical response) was also observed when registering voltammograms in the absence of acid over time. Thus, voltammograms of complex **27** were registered at 0, 5, and 10 min (Figure S18). The formed deposit in the electrode led to a flat voltammogram after 10 min. This behavior is due to electrochemical decomposition of the nanocluster.

CONCLUSIONS

Two series of silicon-supported $[(\mu\text{-}SCH_2)_2N^RFe_2(CO)_6]$ (R = *p*-OHC_6H_4, **3**, and $(CH_2)_2OH$, **4a**, and $(CH_2)_5OH$, **4b**) hydrogenase mimics, as well as POSS-based nanostructures containing eight $[(\mu\text{-}SCH_2)_2N^RFe_2(CO)_6]$ units have been prepared. The first series were synthesized by reaction of the corresponding silyl and silyloxy chlorides and compounds **3** and **4**. The second series was prepared by CuAAC between propargyl derivatives of silyl and silyloxy chlorides and azide **14**. In all cases, the reactions were clean, and the silicon-based $[(\mu\text{-}SCH_2)_2N^RFe_2(CO)_6]$ complexes having up to three [FeFe] units were obtained.

In parallel, the CuAAC of POSS derivative **23a** and azide **14** led to a extremely insoluble triazole derivative that could not be fully characterized. However, the inverse cycloaddition between POSS-derived azide **23b** and $[(\mu\text{-}SCH_2)_2N^RFe_2(CO)_6]$ (R = alkyne) complexes was efficient, leading to POSS-based nanostructures containing eight $[(\mu\text{-}SCH_2)_2N^RFe_2(CO)_6]$ units.

All of the complexes prepared through this work were soluble in organic solvents and hence fully characterizable by spectroscopic media. The data obtained from these complexes may help future research in the heterogenization of these mimics based on $[(\mu\text{-}SCH_2)_2N^RFe_2(CO)_6]$ moieties. Their electrochemistry in the absence of soft acids (AcOH) is similar, with a reduction wave around −1.7 V, which is characteristic of these $[(\mu\text{-}SCH_2)_2N^RFe_2(CO)_6]$ mimics.

However, the behavior of these complexes in the presence of AcOH differs. Complexes **5**−**6b**, **9**−**11**, and **13** lacking 1,2,3-triazole moieties were stable, and their behavior corresponds with analogous $[(\mu\text{-}SCH_2)_2N^RFe_2(CO)_6$; namely, the wave at −1.7 V was scarcely electrocatalytic, while a new electrocatalytic wave around −2.20 V appears. On the contrary, complexes **16** and **18** having two or three CH_2 groups separating the silicon and the 1,2,3-triazole ring evolve into a new complex producing an inverse effect in the current of the wave at −1.7 V. The hydrolyzed product coming from **16** was assigned the structure **16b**. Oppositely, complexes **20**, **22**, and **28** were stable in the presence of AcOH and show the usual electrocatalytic behavior.

Finally, POSS-$[(\mu\text{-}SCH_2)_2N^RFe_2(CO)_6]$ derivatives **25** and **27** show a strong irreversible reduction event and deposit in the electrode either by adding AcOH or by time (successive voltammograms). ^{29}Si NMR shows that the integrity of the silicon cage is not affected by time or AcOH addition.

To conclude, soluble models of silica-based $[(\mu\text{-}SCH_2)_2N^RFe_2(CO)_6]$ mimics have been prepared and their electrochemical properties studied. These synthetic protocols and electrochemical study will be applied in the design of silicon-supported $[(\mu\text{-}SCH_2)_2N^RFe_2(CO)_6]$ mimics.

EXPERIMENTAL SECTION

General Procedure for the Synthesis of Siloxane Derivatives. In an argon-purged flask, Et_3N (4 equiv) and the corresponding alcohol or phenol (1 equiv) were dissolved in Et_2O (4 mL per mmol of phenol **3** or alcohols **4a** and **4b**) at 0 °C. The silyl derivative (1 equiv) was added to the mixture, and the solution was stirred at room temperature until total disappearance of the starting materials by thin-layer chromatography (TLC). The solvent was partially removed under vacuum, and the concentrated solution was filtered to eliminate triethylammonium chloride. The remaining solvent was then evaporated, and the crude products were purified by SiO_2 chromatography.

Synthesis of ***5****.* Following the general procedure, a solution of Et_3N (0.17 mL, 1.25 mmol, 4 equiv) and **3** (300 mg, 0.60 mmol, 2 equiv) in Et_2O (2.4 mL) at 0 °C was treated with dichlorodiphenylsilane (80 mg, 0.30 mmol, 1 equiv). The reaction mixture was stirred for 1 h. The crude obtained after workup was purified by SiO_2 chromatography (Hex/EtOAc = 9/1) to yield pure **5** as a red solid (186 mg, 52%): ^{1}H NMR (300 MHz, $CDCl_3$) δ 7.75 (d, J = 6.9 Hz, 4H,

https://doi.org/10.1021/acs.organomet.2c00277
Organometallics XXXX, XXX, XXX−XXX

CH_{arom}), 7.57−7.31 (m, 6H, CH_{arom}), 6.93 (d, J = 8.5 Hz, 4H, CH_{arom}), 6.58 (d, J = 8.5 Hz, 4H, CH_{arom}), 4.24 (s, 8H, NCH_2S); ^{13}C NMR (75 MHz, $CDCl_3$) δ 207.1 (CO), 148.1 (C), 139.9 (C), 135.1 (CH), 131.2 (C), 131.0 (CH), 128.1 (CH), 120.9 (CH), 117.4 (CH), 50.3 (CH_2); ^{29}Si NMR (99 MHz, $CDCl_3$) δ −37.40; IR ($CHCl_3$) ν 2073 (CO), 2031 (CO), 1993 (CO) cm^{-1}; ESI-HRMS m/z calcd for $C_{40}H_{27}Fe_4N_2O_{14}S_4Si$ $[M + H]^+$ 1138.75241; found 1138.75115.

Synthesis of ***6a***. Following the general procedure, a solution of Et_3N (0.16 mL, 1.16 mmol, 4 equiv) and **4a** (250 mg, 0.58 mmol, 2 equiv) in Et_2O (2.4 mL) at 0 °C was treated with dichlorodiphenylsilane (73 mg, 0.29 mmol, 1 equiv). The reaction mixture was stirred for 1 h. The crude obtained after workup was purified by SiO_2 chromatography. (Hex/EtOAc = 9/1) to yield pure **6a** as a red solid (160 mg, 53%): ^1H NMR (500 MHz, $CDCl_3$) δ 7.50 (m, 6H, CH_{arom}), 7.41 (t, J = 7.4 Hz, 4H, CH_{arom}), 3.59 (t, J = 5.5 Hz, 4H, OCH_2), 3.56 (s, 8H, NCH_2S), 2.89 (t, J = 5.5 Hz, 4H, CH_2); ^{13}C NMR (75 MHz, $CDCl_3$) δ 207.7 (CO), 134.6 (CH), 131.4 (C), 130.8 (CH), 128.1 (CH), 61.4 (OCH_2), 58.6 (NCH_2), 53.5 (NCH_2S); ^{29}Si NMR (99 MHz, $CDCl_3$) δ −30.10; IR ($CHCl_3$) ν 2071 (CO), 2027 (CO), 1989 (CO) cm^{-1}; ESI-HRMS m/z calcd for $C_{32}H_{27}Fe_4N_2O_{14}S_4Si$ $[M + H]^+$ 1042.75104; found 1042.74807.

Synthesis of ***6b***. Following the general procedure, a solution of Et_3N (0.15 mL, 1.05 mmol, 4 equiv) and **4b** (250 mg, 0.53 mmol, 2 equiv) in Et_2O (2.4 mL) at 0 °C was treated with dichlorodiphenylsilane (63 mg, 0.26 mmol, 1 equiv). The reaction mixture was stirred for 1 h. The crude obtained after workup was purified by SiO_2 chromatography (Hex/EtOAc = 9/1) to yield pure **6b** as a red solid (164 mg, 56%): ^1H NMR (300 MHz, $CDCl_3$) δ 7.61 (d, J = 6.2 Hz, 4H, CH_{arom}), 7.52−7.32 (m, 6H, CH_{arom}), 3.72 (t, J = 6.4 Hz, 4H, OCH_2), 3.46 (s, 8H, NCH_2S), 2.59 (d, J = 6.8 Hz, 4H, NCH_2), 1.53 (p, J = 6.4 Hz, 4H, CH_2), 1.40−1.10 (m, 8H, CH_2); ^{13}C NMR (75 MHz, $CDCl_3$) δ 207.9 (CO), 134.9 (CH), 133.0 (C), 130.4 (CH), 128.0 (CH), 62.9 (OCH_2), 57.3 (NCH_2), 53.1 (NCH_2S), 32.1 (CH_2), 27.4 (CH_2), 23.2 (CH_2); ^{29}Si NMR (99 MHz, $CDCl_3$) δ −32.20; IR ($CHCl_3$) ν 2071 (CO), 2028 (CO), 1990 (CO) cm^{-1}; ESI-HRMS m/z calcd for $C_{38}H_{39}Fe_4N_2O_{14}S_4Si$ $[M + H]^+$ 1126.84503; found 1126.84478.

Synthesis of ***9***. Following the general procedure, a solution of Et_3N (0.13 mL, 0.96 mmol, 4 equiv) and **4a** (200 mg, 0.46 mmol, 2 equiv) in Et_2O (2 mL) at 0 °C was treated with 1,3-dichloro-1,1,3,3-tetramethyldisiloxane (47 mg, 0.23 mmol, 1 equiv). The reaction mixture was stirred for 1 h. The crude obtained after workup was purified by SiO_2 chromatography (Hex/EtOAc = 7/3) to yield pure **9** as a red solid (110 mg, 48%): ^1H NMR (300 MHz, $CDCl_3$) δ 3.65 (s, 8H, NCH_2S), 3.51 (t, J = 5.4 Hz, 4H, OCH_2), 2.86 (t, J = 5.4 Hz, 4H, NCH_2), 0.06 (s, 12H, CH_3Si); ^{13}C NMR (75 MHz, $CDCl_3$) δ 207.9 (CO), 60.8 (OCH_2), 59.1 (NCH_2), 53.8 (NCH_2S), −1.0 (CH_3Si); ^{29}Si NMR (99 MHz, $CDCl_3$) δ −10.95; IR ($CHCl_3$) ν 2071 (CO), 2027 (CO), 1985 (CO) cm^{-1}; ESI-HRMS m/z calcd for $C_{24}H_{29}Fe_4N_2O_{15}S_4Si_2$ $[M + H]^+$ 992.74318; found 992.73848.

Synthesis of ***10***. Following the general procedure, a solution of Et_3N (0.18 mL, 1.40 mmol, 4 equiv) and **4a** (300 mg, 0.70 mmol, 2 equiv) in Et_2O (2 mL) at 0 °C was treated with 1,7-dichloro-1,1,3,3,5,5,7,7-octamethyltetrasiloxane (122 mg, 0.35 mmol, 1 equiv). The reaction mixture was stirred for 1 h. The crude obtained after workup was purified by SiO_2 chromatography (Hex/EtOAc = 95/5) to yield pure **10** as a red solid (220 mg, 55%): ^1H NMR (300 MHz, $CDCl_3$) δ 3.65 (s, 8H, NCH_2S), 3.53 (t, J = 5.4 Hz, 4H, OCH_2), 2.86 (t, J = 5.4 Hz, 4H, NCH_2), 0.07 (s, 12H, CH_3Si), 0.06 (s, 12H, CH_3Si); ^{13}C NMR (75 MHz, $CDCl_3$) δ 208.0 (CO), 60.7 (OCH_2), 59.3 (NCH_2), 53.8 (NCH_2S), 1.2 (CH_3Si), −1.0 (CH_3Si); ^{29}Si NMR (99 MHz, $CDCl_3$) δ −11.63, −21.11; IR ($CHCl_3$) ν 2072 (CO), 2029 (CO), 1990 (CO) cm^{-1}; ESI-HRMS m/z calcd for $C_{28}H_{41}Fe_4N_2O_{17}S_4Si_4$ $[M + H]^+$ 1140.77622; found 1140.7811.

Synthesis of ***11***. Following the general procedure, a solution of Et_3N (0.10 mL, 0.69 mmol, 4 equiv) and **4a** (150 mg, 0.35 mmol, 3 equiv) in Et_2O (1.4 mL) at 0 °C was treated with trichlorophenylsilane (25 mg, 0.12 mmol, 1 equiv). The reaction mixture was stirred for 1 h. The crude obtained after workup was purified by SiO_2 chromatography (Hex/EtOAc = 8/2) to yield pure **11** as a red solid (78 mg, 48%): ^1H NMR (500 MHz, $CDCl_3$) δ 7.51−7.40 (m, 5H, CH_{arom}), 3.60−3.56 (m, 18 H, OCH_2, NCH_2S), 2.88 (t, J = 5.5 Hz, 6H, CH_2); ^{13}C NMR (126 MHz, $CDCl_3$) δ 207.8 (CO), 134.4 (CH_{arom}), 131.4 (CH_{arom}), 128.8 (C), 128.5 (CH_{arom}), 61.72 (OCH_2), 58.59 (NCH_2), 53.61 (NCH_2S); ^{29}Si NMR (99 MHz, $CDCl_3$) δ −57.50; IR ($CHCl_3$) ν 2071 (CO), 2028 (CO), 1967 (CO) cm^{-1}; ESI-HRMS m/z calcd for $C_{36}H_{30}Fe_6N_3O_{21}S_6Si$ $[M + H]^+$ 1395.5562; found 1395.5558.

Synthesis of ***13***. Following the general procedure, a solution of Et_3N (0.12 mL, 0.98 mmol, 4 equiv) and **3** (230 mg, 0.50 mmol, 2 equiv) in Et_2O (2.0 mL) at 0 °C was treated with (dichloromethylsilyl)ferrocene **12** (74 mg, 0.25 mmol, 1 equiv). The reaction mixture was stirred for 1 h. The crude obtained after workup was purified by SiO_2 chromatography (Hex/EtOAc = 9/1) to yield pure **13** as a red solid (141 mg, 48%): ^1H NMR (300 MHz, $CDCl_3$) δ 7.75 (d, J = 6.9 Hz, 4H, CH_{arom}), 7.57−7.31 (m, 6H, CH_{arom}), 6.93 (d, J = 8.5 Hz, 4H, CH_{arom}), 6.58 (d, J = 8.5 Hz, 4H, CH_{arom}), 4.24 (s, 8H, NCH_2S); ^{13}C NMR (75 MHz, $CDCl_3$) δ 207.1 (CO), 148.1 (C), 139.9 (C), 135.1 (CH), 131.2 (C), 131.0 (CH), 128.1 (CH), 120.9 (CH), 117.4 (CH), 50.3 (CH_2), −3.2 (CH_3Si); ^{29}Si NMR (99 MHz, $CDCl_3$) δ −37.40; IR ($CHCl_3$) ν 2071 (CO), 2028 (CO), 1971 (CO) cm^{-1}; ESI-HRMS m/z calcd for $C_{39}H_{29}Fe_5N_2O_{14}S_4Si$ $[M + H]^+$ 1184.7018; found 1184.6998.

General Procedure for the Synthesis of Triazole Derivatives. In an argon-purged flask, the corresponding alkyne (1 equiv) and the azide (1 equiv per alkyne group) were mixed with $CuSO_4 \cdot 5H_2O$ (1 equiv) and sodium ascorbate (2 equiv). The degassed solvent (1:1 DCM/water mixture, 15 mL per mmol of **14**) was added, and the reaction was stirred at room temperature until disappearance of the starting materials by TLC. The solvent was partially removed under vacuum, and the concentrated solution was extracted with DCM. The organic layer was washed with brine, dried over Na_2SO_4, filtered, and evaporated under reduced pressure. The crude products were purified by SiO_2 chromatography.

Synthesis of ***16***. Following the general procedure, a mixture of **15** (96 mg, 0.30 mmol, 1 equiv), $CuSO_4 \cdot 5H_2O$ (74 mg, 0.30 mmol, 1 equiv), sodium ascorbate (120 mg, 0.60 mmol, 2 equiv), and **14** (300 mg, 0.60 mmol, 2 equiv) in 9 mL of DCM/water (1:1) (9 mL) was stirred for 1 h. After partial evaporation and extraction with DCM, the organic phase was washed with brine, dried over Na_2SO_4, filtered, and concentrated to afford the crude product. Purification by SiO_2 chromatography (Hex/EtOAc = 7/3) yielded pure **16** as a red solid (208 mg, 52%): ^1H NMR (500 MHz, $CDCl_3$) δ 7.77 (s, 2H, N−CH), 7.67−7.53 (m, 8H, CH_{arom}), 7.44−7.33 (m, 6H, CH_{arom}), 6.82 (d, J = 8.8 Hz, 4H, CH_{arom}), 4.34 (s, 8H, N−CH_2), 4.09 (t, J = 6.3 Hz, 4H, CH_2), 3.09 (t, J = 6.3 Hz, 4H, CH_2); ^{13}C NMR (126 MHz, $CDCl_3$) δ 206.9 (CO), 145.6 (C) 144.7 (C), 134.9 (CH_{arom}), 132.4 (C), 130.6 (CH_{arom}), 130.2 (C), 128.1 (CH_{arom}), 122.2 (CH_{arom}), 120.2 (N−CH), 116.4 (CH_{arom}), 62.4 (OCH_2), 49.8 (N−CH_2), 29.2 (CH_2); HMBC ($^{29}Si-^1H$) RMN (500 MHz, $CDCl_3$) δ −31.49; IR ($CHCl_3$) ν 2071 (CO), 2028 (CO), 1967 (CO) cm^{-1}; ESI-HRMS m/z calcd for $C_{48}H_{36}Fe_4N_8O_{14}S_4Si$ $[M + H]^+$ 1328.8479; found 1328.8461.

Synthesis of ***18***. Following the general procedure, a mixture of **17** (104 mg, 0.30 mmol, 1 equiv), $CuSO_4 \cdot 5H_2O$ (74 mg, 0.30 mmol, 1 equiv), sodium ascorbate (120 mg, 0.60 mmol, 2 equiv), and **14** (300 mg, 0.60 mmol, 2 equiv) in 9 mL of DCM/water (1:1) was stirred for 1 h. After partial evaporation and extraction with DCM, the organic phase was washed with brine, dried over Na_2SO_4, filtered, and concentrated to afford the crude product. Purification by SiO_2 chromatography (Hex/EtOAc = 8/2) yielded pure **18** as a red solid (300 mg, 75%): ^1H NMR (500 MHz, $CDCl_3$) δ 7.68−7.58 (m, 10H, CH_{arom}, N−CH), 7.74−7.36 (m, 6H, CH_{arom}), 6.83 (d, J = 8.8 Hz, 4H, CH_{arom}), 4.35 (s, 8H, N−CH_2), 3.90 (t, J = 6.2 Hz, 4H, O−CH_2), 2.92 (t, J = 7.6 Hz, 4H, N−CH_2), 2.02−2.08 (m, 4H, CH_2); ^{13}C NMR (126 MHz, $CDCl_3$) δ 206.9 (CO), 148.3 (C) 144.7 (C), 135.0 (CH_{arom}), 132.8 (C), 130.5 (CH_{arom}), 130.3 (C), 128.0 (CH_{arom}), 122.3 (CH_{arom}), 119.1 (N−CH), 116.3 (CH_{arom}), 62.4 (OCH_2), 49.8 (N−CH_2), 32.0 (CH_2), 22.2 (CH_2); HMBC ($^{29}Si-^1H$) RMN (500 MHz, $CDCl_3$) δ −31.80; IR ($CHCl_3$) ν

https://doi.org/10.1021/acs.organomet.2c00277
Organometallics XXXX, XXX, XXX−XXX

2074 (CO), 2032 (CO), 1993 (CO) cm^{-1}; ESI-HRMS m/z calcd for $C_{50}H_{41}Fe_4N_8O_{14}S_4Si$ $[M + H]^+$ 1356.87933; found 1356.87789.

Synthesis of ***20***. Following the general procedure, a mixture of **19** (48 mg, 0.20 mmol, 1 equiv), $CuSO_4{\cdot}5H_2O$ (50 mg, 0.20 mmol, 1 equiv), sodium ascorbate (80 mg, 0.40 mmol, 2 equiv), and **14** (200 mg, 0.40 mmol, 2 equiv) in 6 mL of DCM/water (1:1) was stirred for 2 h. After partial evaporation and extraction with DCM, the organic phase was washed with brine, dried over Na_2SO_4, filtered, and concentrated to afford the crude product. Purification by SiO_2 chromatography (Hex/EtOAc = 6/4) yielded pure **20** as a red solid (217 mg, 87% yield): ^{1}H NMR (500 MHz, $CDCl_3$) δ 7.95 (s, 2H, N−CH), 7.68 (s, 4H, J = 8.9, CH_{arom}), 6.85 (s, 4H, J = 8.9, CH_{arom}), 4.98 (s, 4H, O−CH_2), 4.34 (s, 8H, N−CH_2), 0.21 (s, 12H, Si−CH_3); ^{13}C NMR (126 MHz, $CDCl_3$) δ 206.9 (CO), 148.4 (C), 144.8 (C), 130.17 (C), 122.4 (CH_{arom}), 120.3 (N−CH), 116.4 (CH_{arom}), 56.9 (O−CH_2), 49.8 (N−CH_2), 0.9 (CH_3); ^{29}Si NMR (99 MHz, $CDCl_3$) δ −9.72; IR ($CHCl_3$) ν 2073 (CO), 2029 (CO), 1984 (CO) cm^{-1}; ESI-HRMS m/z calcd for $C_{38}H_{34}Fe_4N_4O_{15}S_4Si_2$ $[M + H]^+$ 1250.8041; found 1250.7983.

Synthesis of ***22***. Following the general procedure, a mixture of **21** (67 mg, 0.20 mmol, 1 equiv), $CuSO_4{\cdot}5H_2O$ (50 mg, 0.20 mmol, 1 equiv), sodium ascorbate (80 mg, 0.40 mmol, 2 equiv), and **14** (200 mg, 0.40 mmol, 2 equiv) in 6 mL of DCM/water (1:1) was stirred for 3 h. After partial evaporation and extraction with DCM, the organic phase was washed with brine, dried over Na_2SO_4, filtered, and concentrated to afford the crude product. Purification by SiO_2 chromatography (Hex/EtOAc = 6/4) yielded pure **22** as a red solid (210 mg, 78%): ^{1}H NMR (500 MHz, $CDCl_3$) δ 7.92 (s, 2H, N−CH), 7.67 (s, 4H, J = 8.6, CH_{arom}), 6.84 (s, 4H, J = 8.6, CH_{arom}), 5.07 (s, 4H, O−CH_2), 4.42 (s, 2H, CH-Cp), 4.35 (brs, 8H, N−CH_2), 4.27 (s, 2H, CH-Cp), 4.19 (brs, 5H, Cp), 0.52 (s, 3H, Si−CH_3); ^{13}C NMR (126 MHz, $CDCl_3$) δ 206.9 (CO), 148.3 (C), 144.9 (C), 130.1 (C), 122.4 (CH_{arom}), 120.5 (N−CH), 116.4 (CH_{arom}), 73.5 (CH_{cp}), 71.7 (CH_{cp}), 68.8 (C_{cp}), 57.4 (O−CH_2), 49.8 (N−CH_2), −3.3 (Si-CH_3); ^{29}Si NMR (99 MHz, $CDCl_3$) δ −8.05; IR ($CHCl_3$) ν 2074 (CO), 2030 (CO), 1989 (CO) cm^{-1}; ESI-HRMS m/z calcd for $C_{45}H_{34}Fe_5N_8NaO_{14}S_4Si$ $[M + Na]$+ 1368.7491; found 1368.7405

Synthesis of ***25***. Following the general procedure, a mixture of 24 (232 mg, 0.47 mmol, 10 equiv), $CuSO_4{\cdot}5H_2O$ (119 mg, 0.47 mmol, 10 equiv), sodium ascorbate (190 mg, 0.95 mmol, 20 equiv), and **23b** (52 mg, 0.05 mmol, 1 equiv) in 7 mL of DCM/water (1:1) was stirred at room temperature for 6 h. After partial evaporation and extraction with DCM, the organic phase was washed with brine, dried over Na_2SO_4, filtered, and concentrated to afford the crude product. Purification by SiO_2 chromatography (DCM/MeOH = 99/1) yielded pure **25** as a red solid (177 mg, 74%): ^{1}H NMR (500 MHz, $CDCl_3$) δ 7.90 (s, 8H, NCH), 7.81 (d, J = 8.5 Hz, 16H, CH_{arom}), 6.75 (d, J = 8.5 Hz, 16H, CH_{arom}), 4.38−4.34 (m, 16H, CH_2), 4.33 (s, 32H, NCH_2), 2.10−2.02 (m, 16H, CH_2), 0.79−0.56 (m, 16H, $SiCH_2$); ^{13}C NMR (126 MHz, $CDCl_3$) δ 207.0 (CO), 147.4 (CH), 144.4 (C), 127.4 (CH_{arom}), 123.0 (C), 119.6 (C), 116.0 (CH_{arom}), 52.3 (CH_2), 49.7 (NCH_2), 24.1 (CH_2), 8.8 ($SiCH_2$); ^{29}Si NMR (99 MHz, $CDCl_3$) δ −67.2; IR ($CHCl_3$) ν 2070 (CO), 2024 (CO), 1964 (CO) cm^{-1}. Anal. Calcd for $C_{154}H_{127}Fe_{16}N_{32}O_{60}S_{16}Si_8$: C, 35.87; H, 2.55; N, 8.93; S, 10.22. Found: C, 35.77; H, 2.55; N, 8.70; S, 9.70.

Synthesis of ***27***. Following the general procedure, a mixture of **26** (450 mg, 0.87 mmol, 10 equiv), $CuSO_4{\cdot}5H_2O$ (220 mg, 0.87 mmol, 10 equiv), sodium ascorbate (345 mg, 1.74 mmol, 20 equiv), and **23** (95 mg, 0.09 mmol, 1 equiv) in 13 mL of DCM/water (1:1) was stirred at room temperature for 2 h. After partial evaporation and extraction with DCM, the organic phase was washed with brine, dried over Na_2SO_4, filtered, and concentrated to afford the crude product. Purification by SiO_2 chromatography (DCM/MeOH = 99/1) yielded pure **27** as a red solid (400 mg, 88%): ^{1}H NMR (500 MHz, $CDCl_3$) δ 7.74 (s, 8H, N−CH), 6.96 (d, 16H, J = 9.1 Hz, CH_{arom}), 6.68 (d, 16H J = 9.1 Hz, CH_{arom}), 5.13 (s, 16H, CH_2O), 4.35 (t, J = 7.0 Hz, 16H, CH_2), 4.25 (s, 32H, NCH_2), 2.04 (p, J = 7.3 Hz, 16H, CH_2), 0.75−0.59 (m, 16H, $SiCH_2$); ^{13}C NMR (126 MHz, $CDCl_3$) δ 207.1 (CO), 152.7 (C), 144.1 (C), 139.6 (C), 123.4 (CH), 117.7 (CH_{arom}), 116.4 (CH_{arom}), 62.6 (O−CH_2), 52.4 (CH_2), 50.4 (NCH_2), 24.1 (CH_2), 8.8 ($SiCH_2$); ^{29}Si NMR (99 MHz, $CDCl_3$) δ −67.3; IR ($CHCl_3$) ν 2073 (CO), 2033 (CO), 1988 (CO) cm^{-1}. Anal. Calcd for $C_{162}H_{143}Fe_{16}N_{32}O_{68}S_{16}Si_8{\cdot}2CH_2Cl_2$: C, 36.30; H, 2.73; N, 8.26; S, 9.45. Found: C, 36.41; H, 2.69; N, 8.42; S, 9.69.

Synthesis of ***28***. Following the general procedure, a mixture of ethynyltrimethylsilane (40 mg, 0.20 mmol, 1 equiv), $CuSO_4{\cdot}5H_2O$ (119 mg, 0.40 mmol, 1 equiv), sodium ascorbate (236 mg, 0.20 mmol, 2 equiv), and **14** (200 mg, 0.40 mmol, 2 equiv) in 6 mL of DCM/water (1:1) was stirred for 3 h. After partial evaporation and extraction with DCM, the organic phase was washed with brine, dried over Na_2SO_4, filtered, and concentrated to afford the crude product. Purification by SiO_2 chromatography (Hex/EtOAc = 9/1) yielded pure **28** as a red solid (117 mg, 49%): ^{1}H NMR (500 MHz, $CDCl_3$) δ 7.86 (s, 1H, N−CH), 7.68 (d, J = 8.5 Hz, 2H, CH_{arom}), 6.85 (d, J = 8.5 Hz, 2H, CH_{arom}), 4.36 (s, 4H, N−CH_2), 0.38 (s, 9H, Si−CH_3); ^{13}C NMR (126 MHz, $CDCl_3$) δ 206.9 (CO), 147.3 (C), 144.7 (C), 130.1 (C), 127.1 (N−CH), 122.7 (CH_{arom}), 116.4 (CH_{arom}), 49.8 (N−CH_2), −0.9 (Si−CH_3); ^{29}Si NMR (99 MHz, $CDCl_3$) δ −9.43; IR ($CHCl_3$) ν 2073 (CO), 2030 (CO), 1988 (CO) cm^{-1}; ESI-HRMS m/z calcd for $C_{19}H_{18}Fe_2N_4O_6S_2Si$ $[M + H]^+$ 602.9214; found 602.9215.

Electrochemical Studies. Cyclic voltammograms were recorded using a Metrohm model PGSTAT302N Autolab potentiostat with a 3 mm glassy carbon working electrode, 3 M Ag/AgCl as the reference electrode, and a 2 mm Pt-wire counter electrode. All of the measurements were performed at room temperature from CH_3CN or DCM solutions containing 10^{-1} M $[N(^nBu_4)]PF_6$ as the supporting electrolyte, with analyte concentrations of 10^{-3} M (scan rate = 0.1 V/s). All voltammograms are referenced to the $Fc^{0/+}$ system. Unless otherwise stated, the experiments were carried out under an argon atmosphere. When needed, an ultrasound bath was used to promote solubilization in those samples where a suspension was initially obtained.

■ ASSOCIATED CONTENT

Supporting Information

The Supporting Information is available free of charge at https://pubs.acs.org/doi/10.1021/acs.organomet.2c00277.

Preparation of complexes **4b**, **17**, **19**, **21**, **26**, and **18b**; copies of ^{1}H, ^{13}C, ^{29}Si, and IR for the new compounds prepared through this work; Figures S1−S12, procedures for TOF calculations (PDF)

Accession Codes

CCDC 2177156 contains the supplementary crystallographic data for this paper. These data can be obtained free of charge via www.ccdc.cam.ac.uk/data_request/cif, or by emailing data_request@ccdc.cam.ac. uk, or by contacting The Cambridge Crystallographic Data Centre, 12 Union Road, Cambridge CB2 1EZ, UK; fax: + 44 1223336033.

■ AUTHOR INFORMATION

Corresponding Authors

Luis Casarrubios − *Departamento de Química Orgánica, Facultad de Ciencias Químicas, Universidad Complutense, 28040 Madrid, Spain; Centro de Innovación en Química Avanzada (ORFEO−CINQA), Departamento de Química Orgánica, Facultad de Ciencias Químicas, Universidad Complutense, 28040 Madrid, Spain;* orcid.org/0000-0002-9054-3118; Email: lcasarru@ucm.es

Miguel A. Sierra − *Departamento de Química Orgánica, Facultad de Ciencias Químicas, Universidad Complutense, 28040 Madrid, Spain; Centro de Innovación en Química Avanzada (ORFEO−CINQA), Departamento de Química Orgánica, Facultad de Ciencias Químicas, Universidad*

https://doi.org/10.1021/acs.organomet.2c00277
Organometallics XXXX, XXX, XXX−XXX

Complutense, 28040 Madrid, Spain; orcid.org/0000-0002-3360-7795; Email: sierraor@ucm.es

Authors

Sergio Aguado − *Departamento de Química Orgánica, Facultad de Ciencias Químicas, Universidad Complutense, 28040 Madrid, Spain; Centro de Innovación en Química Avanzada (ORFEO−CINQA), Departamento de Química Orgánica, Facultad de Ciencias Químicas, Universidad Complutense, 28040 Madrid, Spain;* orcid.org/0000-0002-3117-0438

Diego J. Vicent − *Departamento de Química Orgánica, Facultad de Ciencias Químicas, Universidad Complutense, 28040 Madrid, Spain; Centro de Innovación en Química Avanzada (ORFEO−CINQA), Departamento de Química Orgánica, Facultad de Ciencias Químicas, Universidad Complutense, 28040 Madrid, Spain*

Carmen Ramírez de Arellano − *Departamento de Química Orgánica, Universidad de Valencia, 46100 Valencia, Spain; Centro de Innovación en Química Avanzada (ORFEO−CINQA), Departamento de Química Orgánica, Facultad de Ciencias Químicas, Universidad Complutense, 28040 Madrid, Spain;* orcid.org/0000-0002-8976-0318

Complete contact information is available at: https://pubs.acs.org/10.1021/acs.organomet.2c00277

Notes

The authors declare no competing financial interest.

■ ACKNOWLEDGMENTS

Support for this work under Grant Nos. PID2019-108429RB-I00 and RED2018-102387-T from the MCINN (Spain) is gratefully acknowledged. M.A.S. thanks the Fundación Ramón Areces for a grant from the XVIII Concurso Nacional de Ayudas a la Investigación en Ciencias de la Vida y de la Materia (CIVP18A3938).

■ DEDICATION

This paper is warmly dedicated to Prof. Brookhart on the occasion of his 80th birthday.

■ REFERENCES

(1) (a) Lubitz, W.; Ogata, H.; Rüdiger, O.; Reijerse, E. Hydrogenases. *Chem. Rev.* **2014**, *114*, 4081−4148. (b) Fontecilla-Camps, J. C.; Volbeda, A.; Cavazza, C.; Nicolet, Y. Structure/Function Relationships of [NiFe]- and [FeFe]-Hydrogenases. *Chem. Rev.* **2007**, *107*, 4273−4303. (c) Vignais, P. M.; Billoud, B. Occurrence, Classification, and Biological Function of Hydrogenases: An Overview. *Chem. Rev.* **2007**, *107*, 4206−4272. (d) del Barrio, M.; Sensi, M.; Orain, C.; Baffert, C.; Dementin, S.; Fourmond, V.; Léger, C. Electrochemical Investigations of Hydrogenases and Other Enzymes That Produce and Use Solar Fuels. *Acc. Chem. Res.* **2018**, *51*, 769−777. (e) Greene, B. L. Progress and Opportunities in Photochemical Enzymology of Oxidoreductases. *ACS Catal.* **2021**, *11*, 14635−14650. (f) Morra, S. Fantastic [FeFe]-Hydrogenases and Where to Find Them. *Front. Microbiol.* **2022**, *13*, 853626. (g) Stripp, S. T.; Duffus, B. R.; Fourmond, V.; Léger, C.; Leimkühler, S.; Hirota, S.; Hu, Y.; Jasniewski, A.; Ogata, H.; Ribbe, M. W. Second and Outer Coordination Sphere Effects in Nitrogenase, Hydrogenase, Formate Dehydrogenase, and CO Dehydrogenase. *Chem. Rev.* **2022**, *122*, 11900−11973. (h) Amanullah, S.; Saha, P.; Nayek, A.; Ahmed, M. E.; Dey, A. Biochemical and artificial pathways for the reduction of carbon dioxide, nitrite and the competing proton reduction: effect of 2nd sphere interactions in catalysis. *Chem. Soc. Rev.* **2021**, *50*, 3755−3823.

(2) Birrell, J. A.; Rodriguez-Macia, P.; Reijerse, E. J.; Martini, M. A.; Lubitz, W. The catalytic cycle of [FeFe] hydrogenase: A tale of two sites. *Coord. Chem. Rev.* **2021**, *449*, 214191.

(3) (a) Li, Y.; Rauchfuss, T. B. Synthesis of Diiron(I) Dithiolato Carbonyl Complexes. *Chem. Rev.* **2016**, *116*, 7043−7077. (b) Amaro-Gahete, J.; Pavliuk, M. V.; Tian, H.; Esquivel, D.; Romero-Salguero, F. J.; Ott, S. Catalytic systems mimicking the [FeFe]-hydrogenase active site for visible-light-driven hydrogen production. *Coord. Chem. Rev.* **2021**, *448*, 214172−214206. (c) Gómez-Gallego, M.; Sierra, M. A. Deuteration mechanistic studies of hydrogenase mimics. *Inorg. Chem. Front.* **2021**, *8*, 3934−3950. (d) Schilter, D.; Camara, J. M.; Huynh, M. T.; Hammes-Schiffer, S.; Rauchfuss, T. B. Hydrogenase enzymes and their synthetic models: The role of metal hydrides. *Chem. Rev.* **2016**, *116*, 8693−8749. (e) Prasad, P.; Selvan, D.; Chakraborty, S. Biosynthetic Approaches towards the Design of Artificial Hydrogen-Evolution Catalysts. *Chem.—Eur. J.* **2020**, *26*, 12494−12509. (f) Wang, F.; Wang, W.-G.; Wang, H.-Y.; Si, G.; Tung, C. H.; Wu, L.-Z. Artificial Photosynthetic Systems Based on [FeFe]-Hydrogenase Mimics: the Road to High Efficiency for Light-Driven Hydrogen Evolution. *ACS Catal.* **2012**, *2*, 407−416. (g) Kleinhaus, J. T.; Wittkamp, F.; Yadav, S.; Siegmund, D.; Apfel, U.-P. [FeFe]-Hydrogenases: maturation and reactivity of enzymatic systems and overview of biomimetic models. *Chem. Soc. Rev.* **2021**, *50*, 1668−1784.

(4) (a) Cuendet, P.; Rao, K. K.; Grätzel, M.; Hall, D. O. Light induced H_2 evolution in a hydrogenase-TiO_2 particle system by direct electron transfer or via rhodium complexes. *Biochimie* **1986**, *68*, 217−21. (b) Reisner, E.; Fontecilla-Camps, J. C.; Armstrong, F. A. Catalytic electrochemistry of a [NiFeSe]-hydrogenase on TiO_2 and demonstration of its suitability for visible-light driven H_2 production. *Chem. Commun.* **2009**, *5*, 550−552. (c) Reisner, E.; Powell, D. J.; Cavazza, C.; Fontecilla-Camps, J. C.; Armstrong, F. A. Visible Light-Driven H_2 Production by Hydrogenases Attached to Dye-Sensitized TiO_2 Nanoparticles. *J. Am. Chem. Soc.* **2009**, *131*, 18457−18466. (d) Bae, S.; Shim, E.; Yoon, J.; Joo, H. Photoanodic and cathodic role of anodized tubular titania in light-sensitized enzymatic hydrogen production. *J. Power Sources* **2008**, *185*, 439−444.

(5) (a) Alonso-Lomillo, M. A.; Rüdiger, O.; Maroto-Valiente, A.; Velez, M.; Rodríguez-Ramos, I.; Muñoz, F. J.; Fernández, V. M.; De Lacey, A. L. Hydrogenase-coated carbon nanotubes for efficient H_2 oxidation. *Nano Lett.* **2007**, *7*, 1603−1608. (b) Blackburn, J. L.; Svedruzic, D.; McDonald, T. J.; Kim, Y.-H.; King, P. W.; Heben, M. J. Raman spectroscopy of charge transfer interactions between single wall carbon nanotubes and [FeFe] hydrogenase. *Dalton Trans.* **2008**, *40*, 5454−5461. (c) McDonald, T. J.; Svedruzic, D.; Kim, Y.-H.; Blackburn, J. L.; Zhang, S. B.; King, P. W.; Heben, M. J. Wiring-Up Hydrogenase with Single-Walled Carbon Nanotubes. *Nano Lett.* **2007**, *7*, 3528−3534. (d) Brown, K. A.; Dayal, S.; Ai, X.; Rumbles, G.; King, P. W. Controlled assembly of hydrogenase-CdTe nanocrystal hybrids for solar hydrogen production. *J. Am. Chem. Soc.* **2010**, *132*, 9672−9680.

(6) (a) Pullen, S.; Fei, H.; Orthaber, A.; Cohen, S. M.; Ott, S. Enhanced Photochemical Hydrogen Production by a Molecular Diiron Catalyst Incorporated into a Metal−Organic Framework. *J. Am. Chem. Soc.* **2013**, *135*, 16997−17003. (b) Pullen, S.; Roy, S.; Ott, S. [FeFe] Hydrogenase active site model chemistry in a UiO-66 metal−organic framework. *Chem. Commun.* **2017**, *53*, 5227−5230. (c) Castner, A. T.; Johnson, B. A.; Cohen, S. M.; Ott, S. Mimicking the Electron Transport Chain and Active Site of [FeFe] Hydrogenases in One Metal−Organic Framework: Factors That Influence Charge Transport. *J. Am. Chem. Soc.* **2021**, *143*, 7991−7999.

(7) Yu, T.; Zeng, Y.; Chen, J.; Li, Y. Y.; Yang, G.; Li, Y. Exceptional dendrimer-based mimics of diiron hydrogenase for the photochemical production of hydrogen. *Angew. Chem., Int. Ed. Engl.* **2013**, *52*, 5631−5635.

(8) (a) Wang, F.; Liang, W.-J.; Jian, J.-X.; Li, C.-B.; Chen, B.; Tung, C.-H.; Wu, L.-Z. Exceptional Poly(acrylic acid)-Based Artificial [FeFe]-Hydrogenases for Photocatalytic H 2 Production in Water. *Angew. Chem., Int. Ed.* **2013**, *52*, 8134−8138. (b) Liang, W.-J.; Wang,

F.; Wen, M.; Jian, J-X.; Wang, X.-Z.; Chen, B.; Tung, C.-H.; Wu, L. Z. Branched Polyethylenimine Improves Hydrogen Photoproduction from a CdSe Quantum Dot/[FeFe]-Hydrogenase Mimic System in Neutral Aqueous Solutions. *Chem.—Eur. J.* **2015**, *21*, 3187−3192.
(9) Wang, H.-Y.; Wang, W.-G.; Si, G.; Wang, F.; Tung, C.-H.; Wu, L.-Z. Photocatalytic Hydrogen Evolution from Rhenium(I) Complexes to [FeFe] Hydrogenase Mimics in Aqueous SDS Micellar Systems: A Biomimetic Pathway. *Langmuir* **2010**, *26*, 9766−9771.
(10) Nann, T.; Ibrahim, S. K.; Woi, P.-M.; Xu, S.; Ziegler, J.; Pickett, C. J. Water Splitting by Visible Light: A Nanophotocathode for Hydrogen Production. *Angew. Chem., Int. Ed.* **2010**, *49*, 1574−1577.
(11) Kluwer, A. M.; Kapre, R.; Hartl, F.; Lutz, M.; Spek, A. L.; Brouwer, A. M.; van Leeuwen, P. W. N. M.; Reek, J. N. H. Self-assembled biomimetic [2Fe2S]-hydrogenase-based photocatalyst for molecular hydrogen evolution. *Proc. Natl. Acad. Sci. U.S.A.* **2009**, *106*, 10460−10465.
(12) Williams, W. B.; Nash, A.; Yamamoto, N.; Patrick, M.; Tran, I. C.; Gu, J. Unraveling Activity and Decomposition Pathways of [FeFe] Hydrogenase Mimics Covalently Bonded to Silicon Photoelectrodes. *Adv. Mater. Interfaces* **2021**, *8*, 2001961.
(13) Wang, W.; Yu, T.; Zeng, Y.; Chen, J.; Li, Y. An [Fe-Fe]-Hydrogenase Mimic Immobilized on MCM-41 for the Photochemical Production of Hydrogen in Pure Water. *Chin. J. Chem.* **2014**, *32* (6), 479−484.
(14) Wang, W.; Yu, T.; Zeng, Y.; Chen, J.; Yang, G.; Li, Y. Enhanced photocatalytic hydrogen production from an MCM-41-immobilized photosensitizer-[Fe-Fe] hydrogenase mimic dyad. *Photochem. Photobiol. Sci.* **2014**, *13* (11), 1590−1597.
(15) (a) Buday, P.; Kasahara, C.; Hofmeister, E.; Kowalczyk, D.; Farh, M. K.; Riediger, S.; Schulz, M.; Wächtler, M.; Furukawa, S.; Saito, M.; Ziegenbalg, D.; Gräfe, S.; Bäuerle, P.; Kupfer, S.; Dietzek-Ivanšić, B.; Weigand, W. Activating a [FeFe] Hydrogenase Mimic for Hydrogen Evolution under Visible Light. *Angew. Chem., Int. Ed.* **2022**, e202202079. (b) Petuker, A.; Reback, M. L.; Apfel, U.-P. Carbon/Silicon Exchange at the Apex of Diphos- and Triphos-Derived Ligands - More Than Just a Substitute? *Eur. J. Inorg. Chem.* **2017**, *2017*, 3295−3301.
(16) Goy, R.; Bertini, L.; Görls, H.; De Gioia, L.; Talarmin, J.; Zampella, G.; Schollhammer, P.; Weigand, W. Silicon-Heteroaromatic [FeFe] hydrogenase model complexes: insight into protonation, electrochemical properties, and molecular structures. *Chemistry* **2015**, *21*, 5061−5073 and references therein.
(17) Apfel, U.-P.; Troegel, D.; Halpin, Y.; Tschierlei, S.; Uhlemann, U.; Görls, H.; Schmitt, M.; Popp, J.; Dunne, P.; Venkatesan, M.; Coey, M.; Rudolph, M.; Vos, J. G.; Tacke, R.; Weigand, W. Models for the Active Site in [FeFe] Hydrogenase with Iron-Bound Ligands Derived from Bis-, Tris-, and Tetrakis(mercaptomethyl)silanes. *Inorg. Chem.* **2010**, *49*, 10117−10132.
(18) Goy, R.; Apfel, U.-P.; Elleouet, C.; Escudero, D.; Elstner, M.; Gorls, H.; Talarmin, J.; Schollhammer, P.; Gonzalez, L.; Weigand, W. A Silicon-Heteroaromatic System as Photosensitizer for Light-Driven Hydrogen Production by Hydrogenase Mimics. *Eur. J. Inorg. Chem.* **2013**, *2013*, 4466−4472.
(19) Groom, C. R.; Bruno, I. J.; Lightfoot, M. P.; Ward, S. C. The Cambridge Structural Database. *Acta Crystallogr.* **2016**, *B72*, 171−179.
(20) Tard, C.; Pickett, C. J. Structural and Functional Analogues of the Active Sites of the [Fe]-, [NiFe]-, and [FeFe]-Hydrogenases. *Chem. Rev.* **2009**, *109*, 2245−2274.
(21) Herberhold, M.; Ayazi, A.; Milius, W.; Wrackmeyer, B. Silyl derivatives of ferrocene with pending indenyl or fluorenyl substituents at silicon. *J. Organomet. Chem.* **2002**, *656*, 71−80.
(22) Merinero, A. D.; Collado, A.; Casarrubios, L.; Gómez-Gallego, M.; Ramírez de Arellano, C.; Caballero, A.; Zapata, F.; Sierra, M. A. *Inorg. Chem.* **2019**, *58*, 16267−16278.
(23) El Aziz, Y.; Mehrban, N.; Taylor, P. G.; Birchall, M. A.; Bowen, J.; Bassindale, A. R.; Pitak, M. B.; Coles, S. J. Facile synthesis of novel hybrid POSS biomolecules via "Click" reactions. *RSC Adv.* **2017**, *7*, 37474−37477.
(24) (a) Cordes, D. B.; Lickiss, P. D.; Rataboul, F. Recent developments in the chemistry of cubic polyhedral oligosilsesquioxanes. *Chem. Rev.* **2010**, *110*, 2081−2173. (b) Baney, R. H.; Itoh, M.; Sakakibara, A.; Suzuki, T. Silsesquioxanes. *Chem. Rev.* **1995**, *95*, 1409−1430.
(25) Recent examples: (a) Shi, H.; Yang, J.; You, M.; Li, Z.; He, C. Polyhedral Oligomeric Silsesquioxanes (POSS)-Based Hybrid Soft Gels: Molecular Design, Material Advantages, and Emerging Applications. *ACS Mater. Lett.* **2020**, *2*, 296−316. (b) Du, Y.; Liu, H. Cage-like silsesquioxanes-based hybrid materials. *Dalton Trans.* **2020**, *49*, 5396−5405.
(26) Examples: (a) Vautravers, N. R.; André, P.; Cole-Hamilton, D. J. Fluorescence Activation of a Polyhedral Oligomeric Silsesquioxane in the Presence of Reducing Agents. *J. Mater. Chem.* **2009**, *19*, 4545−4550. (b) Vautravers, N. R.; André, P.; Slawin, A. M. Z.; Cole-Hamilton, D. J. Synthesis and Characterization of Photoluminescent Vinylbiphenyl Decorated Polyhedral Oligomeric Silsesquioxanes. *Org. Biomol. Chem.* **2009**, *7*, 717−724.
(27) (a) Żak, P.; Dudziec, B.; Kubicki, M.; Marciniec, B. Silylative Coupling versus Metathesis − Efficient Methods for the Synthesis of Difunctionalized Double-Decker Silsesquioxane Derivatives. *Chem.—Eur. J.* **2014**, *20*, 9387−9393. (b) Żak, P.; Pietraszuk, C. Application of Olefin Metathesis in the Synthesis of Functionalized Polyhedral Oligomeric Silsesquioxanes (POSS) and POSS-Containing Polymeric Materials. *Beilstein J. Org. Chem.* **2019**, *15*, 310−332. (c) Żak, P.; Pietraszuk, C.; Marciniec, B.; Spólnik, B.; Danikiewicz, W. Efficient Functionalisation of Cubic Monovinylsilsesquioxanes via Cross-Metathesis and Silylative Coupling with Olefins in the Presence of Ruthenium Complexes. *Adv. Synth. Catal.* **2009**, *351*, 2675−2682.
(28) Grzelak, M.; Januszewski, R.; Marciniec, B. Synthesis and Hydrosilylation of Vinyl-Substituted Open-Cage Silsesquioxanes with Phenylsilanes: Regioselective Synthesis of Trifunctional Silsesquioxanes. *Inorg. Chem.* **2020**, *59*, 7830−7840.
(29) Fabritz, S.; Heyl, D.; Bagutski, V.; Empting, M.; Rikowski, E.; Frauendorf, H.; Balog, I.; Fessner, W.-D.; Schneider, J. J.; Avrutina, O.; Kolmar, H. Towards click bioconjugations on cube-octameric silsesquioxane scaffolds. *Org. Biomol. Chem.* **2010**, *8*, 2212−2218.
(30) Ahmed, E. M.; Dey, S.; Mondal, B.; Dey, A. H_2 evolution catalyzed by a FeFe-hydrogenase synthetic model covalently attached to graphite surfaces. *Chem. Commun.* **2017**, *53*, 8188−8191.
(31) (a) Wang, Z.; Li, Y.; Dong, X.-H.; Yu, X.; Guo, K.; Su, H.; Yue, K.; Wesdemiotis, C.; Cheng, S. Z. D.; Zhang, W.-B. Giant gemini surfactants based on polystyrene−hydrophilic polyhedral oligomeric silsesquioxane shape amphiphiles: sequential "click" chemistry and solution self-assembly. *Chem. Sci.* **2013**, *4*, 1345−1352. (b) Su, H.; Zheng, J.; Wang, Z.; Lin, F.; Feng, X.; Dong, X.-H.; Becker, M. L.; Cheng, S. Z. D.; Zhang, W.-B.; Li, Y. Sequential Triple "Click" Approach toward Polyhedral Oligomeric Silsesquioxane-Based Multi-headed and Multitailed Giant Surfactants. *ACS Macro Lett.* **2013**, *2*, 645−650. (c) Tinmaz, H. B.; Arslan, I.; Tasdelen, M. A. Star polymers by photoinduced copper-catalyzed azide-alkyne cycloaddition click chemistry. *J. Polym. Sci., Part A: Polym. Chem.* **2015**, *53*, 1687−1695. (d) Trastoy, B.; Bonsor, D. A.; Perez-Ojeda, M. E.; Jimeno, M. L.; Mendez-Ardoy, A.; Garcia-Fernandez, J. M.; Sundberg, E. J.; Chiara, J. L. Synthesis and Biophysical Study of Disassembling Nanohybrid Bioconjugates with a Cubic Octasilsesquioxane Core. *Adv. Funct. Mater.* **2012**, *22*, 3191−3201. (e) Zhang, W.-B.; Tu, Y.; Ranjan, R.; Van Horn, R. M.; Leng, S.; Wang, J.; Polce, M. J.; Wesdemiotis, C.; Quirk, R. P.; Newkome, G. R.; Cheng, S. Z. D. Clicking" Fullerene with Polymers: Synthesis of [60]Fullerene End-Capped Polystyrene. *Macromolecules* **2008**, *41*, 515−517.
(32) (a) Becker, R.; Amirjalayer, S.; Li, P.; Woutersen, S.; Reek, J. N. H. An iron-iron hydrogenase mimic with appended electron reservoir for efficient proton reduction in aqueous media. *Sci. Adv.* **2016**, *2*, e1501014. (b) Fan, H.-J.; Hall, M. B. A Capable Bridging Ligand for Fe-Only Hydrogenase: Density Functional Calculations of a Low-Energy Route for Heterolytic Cleavage and Formation of Dihydrogen. *J. Am. Chem. Soc.* **2001**, *123*, 3828−3829. (c) Schwartz, L.; Eilers, G.; Eriksson, L.; Gogoll, A.; Lomoth, R.; Ott, S. Iron hydrogenase active

https://doi.org/10.1021/acs.organomet.2c00277
Organometallics XXXX, XXX, XXX−XXX

site mimic holding a proton and a hydride. *Chem. Commun.* **2006**, *5*, 520−522. (d) Eilers, G.; Schwartz, L.; Stein, M.; Zampella, G.; de Gioia, L.; Ott, S.; Lomoth, R. Ligand versus metal protonation of an iron hydrogenase active site mimic. *Eur. J. Chem.* **2007**, *13*, 7075−7084. (e) Wang, F.; Wang, M.; Liu, X.; Jin, K.; Dong, W.; Sun, L. Protonation, electrochemical properties and molecular structures of halogen-functionalized diiron azadithiolate complexes related to the active site of iron-only hydrogenases. *Dalton Trans.* **2007**, *34*, 3812−3819.

(33) Eckermann, A. L.; Feld, D. J.; Shaw, J. A.; Meade, T. J. Electrochemistry of redox-active self-assembled monolayers. *Coord. Chem. Rev.* **2010**, *254*, 1769−1802.

(34) Felton, G. A. N.; Vannucci, A. K.; Chen, J.; Lockett, L. T.; Okumura, N.; Petro, B. J.; Zakai, U. I.; Evans, D. H.; Glass, R. S.; Lichtenberger, D. L. Hydrogen Generation from Weak Acids: Electrochemical and Computational Studies of a Diiron Hydrogenase Mimic. *J. Am. Chem. Soc.* **2007**, *129*, 12521−12530.

(35) Complex **16** also evolves spontaneously to the new compound **16b** in solution of $CDCl_3$. See the SI.

https://doi.org/10.1021/acs.organomet.2c00277
Organometallics XXXX, XXX, XXX−XXX